ACS NANO

www.acsnano.org

Reconfigurable Chirality of DNA-Bridged Nanorod Dimers

Brian Hyun-jong Lee, Nicholas A. Kotov, and Gaurav Arya*

Cite This: *ACS Nano* 2021, 15, 13547−13558

Read Online

ACCESS | Metrics & More | Article Recommendations | SI Supporting Information

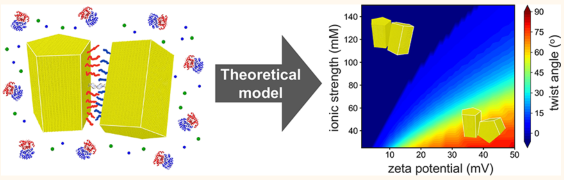

ABSTRACT: **Gold nanorods assembled in a side-by-side chiral configuration have potential applications in sensing due to their strong chiroptical surface plasmon resonances. Recent experiments have shown that dimers of gold nanorods bridged by double-stranded DNA exhibit variable chiral configurations depending on the chemical and ionic properties of the solvent medium. Here, we uncover the underlying physics governing this intriguing chiral behavior of such DNA-bridged nanorods by theoretically evaluating their configurational free energy landscape. Our results reveal how chiral configurations emerge from an interplay between the twist−stretch coupling of the intervening DNA and the intermolecular interactions between the nanorods, with dimers exhibiting left-handed chirality when the interparticle interactions are dominated by attractive depletion or van der Waals forces and right-handed chirality when dominated by repulsive electrostatic or steric forces. We demonstrate how changes in the depletant or ion concentration of the solvent medium lead to different classes of configurational responses by the dimers, including chirality-switching behavior, in good agreement with experimental observations. Based on extensive analyses of how material properties like nanorod aspect ratio, DNA length, and graft height modulate the free energy landscape, we propose strategies for tuning the environmentally responsive reconfigurability of the nanorod dimers. Overall, this work should help control the chirality and related optical activity of nanoparticle dimers and higher-order assemblies for various applications.**

KEYWORDS: *gold nanorods, chirality, DNA-mediated assembly, twist−stretch coupling, plasmonic nanoparticles, ion concentration, zeta potential*

Chiral nanostructures formed by inorganic nanoparticles have potential applications in nanosensing,[1,2] chiral catalysis,[3−6] cellular stimulation,[7] drug discovery,[8] nanoscale machines,[9,10] and optical metamaterials.[11,12] Gold nanorods (AuNRs) in particular are popular building blocks for creating such chiral structures, as their longitudinal surface plasmon resonance in the visible and near-infrared region along with their biocompatibility makes them useful candidates for biological applications.[13,14] Because of the elongated shapes of these particles, chiral structures can be fabricated simply by assembling the AuNRs in a side-by-side arrangement in which the rods exhibit either a negative or a positive twist angle ϕ between their longitudinal axes ($0° < |\phi| < 90°$) to produce left- or right-handed chirality, respectively. Such chiral arrangements have been achieved by bridging the AuNRs with organic materials like polymers,[15] proteins,[16,17] nucleic acids,[18−23] or templates such as DNA origami.[9,10,24−27] Among these, AuNR dimers bridged by a single piece of double-stranded DNA (dsDNA) have been particularly useful as biosensors with low detection limits due to the exceptionally strong chiroptical activity in the part of the electromagnetic spectrum where biomolecules display little to no polarization rotation. Unlike AuNRs assembled on templates, these dimers were able to penetrate into cells and can potentially be scalably produced through self-assembly.[20,22,23] In addition, unlike the particles bridged by polymers or proteins, AuNR dimers bridged by dsDNA displayed intriguing changes in their configuration and chirality, often accompanied by drastic shifts in their circular dichroism, depending on the presence of biological analytes and whether the dimers were present in intra- or extracellular environment.

While these studies have demonstrated the potential of AuNR dimers bridged by dsDNA as nanosensors, the underlying mechanism for their chiral assembly configuration and their medium-dependent switch in chirality observed experimentally is not well understood. One possible source of these behaviors is the twist−stretch coupling of the bridging dsDNA: because of its handedness, dsDNA is a chiral molecule that prefers to underwind when it is compressed and overwind

Received: May 21, 2021
Accepted: July 20, 2021
Published: July 22, 2021

https://doi.org/10.1021/acsnano.1c04326

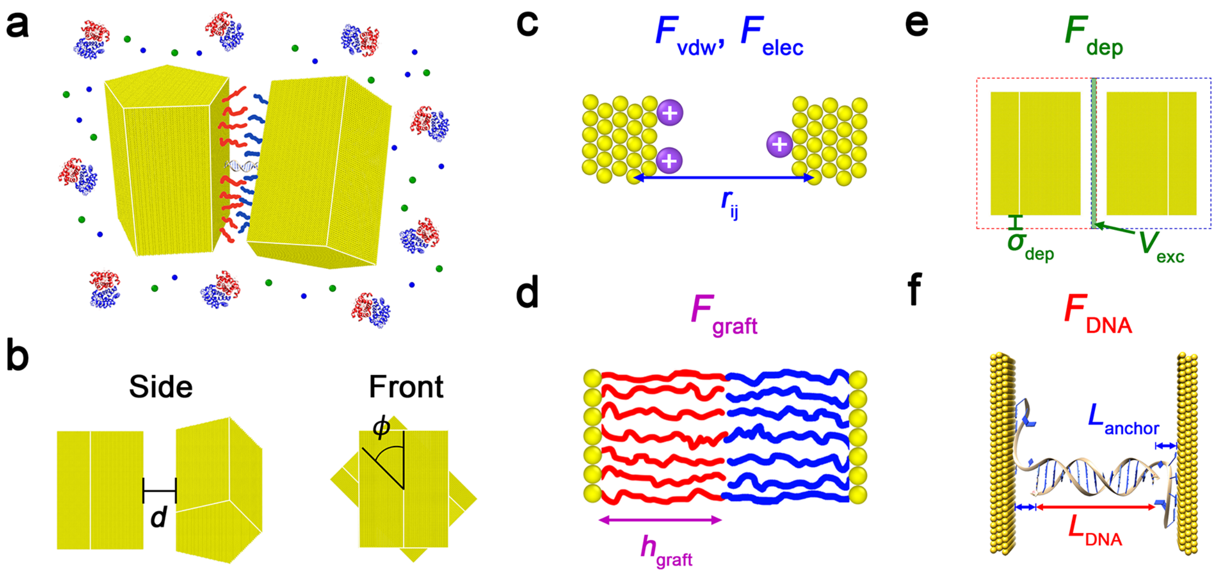

Figure 1. Schematics showing the configuration and energetic interactions of the AuNR dimer system. (a) Polymer-grafted gold nanorods are bridged by dsDNA and present in a solvent medium containing macromolecules and salt. For clarity, polymer chains attached to the rods are shown in different colors, and only those chains attached to the interacting facets are shown. (b) Interparticle configuration of the dimers is well described by *d* and ϕ. (c−f) Free energy of this dimer system contains contributions from vdW and electrostatic interactions between the rods (c), steric repulsion of the grafted polymers (d), depletion attraction (e), and elastic energy of dsDNA (f). Note that the penta-twinned geometry of AuNRs is chosen here as an example. The model is equally applicable to AuNRs with other faceted geometries.

when it is stretched.[28] This suggests that while the nanorods on their own should not prefer any particular handedness, AuNR dimers will prefer the negative twist angle when the intervening DNA is in a compressed state and positive twist angle with stretched DNA. The configuration of the bridged DNA, and of the nanorods, must then depend on the interplay between interparticle forces acting between the nanorods and mechanical resistance of the bridging dsDNA itself. For AuNR systems, the relevant interparticle forces include van der Waals (vdW) and electrostatic interactions acting between the rods, steric interactions between polymer chains grafted onto the rods to stabilize them, and depletion forces arising from macromolecules present in the solvent. Hence, we can conjecture that the medium-dependent chirality of AuNR dimers observed experimentally is related to changes in one or more of these interparticle interactions brought about by changes in solvent conditions, which then affects the twist of the bridging dsDNA. Indeed, experiments have shown that changes in the concentration of ions and macromolecules present in the solvent[16,22] and the capping agent on nanorods,[20] each of which affect the interactions between the nanorods, are accompanied by changes in the configuration of the assembled AuNRs. How these various interactions vary with the environment and material properties of the nanorods to produce known—and potentially unexplored—AuNR configurations also remains unknown.

In this study, we investigate the underlying physics governing the self-assembled configuration of AuNR dimers bridged by dsDNA and propose guidelines for controlling the configuration. In particular, we develop a theoretical model for estimating the interaction free energy of AuNR dimers that incorporates all the aforementioned components of interparticle interactions and analyze the configuration-dependent free energy landscape of the dimers as a function of solvent conditions and material properties. Our analysis reveals that the chirality switch can indeed spontaneously occur due to changes in solvent conditions tilting the balance between attractive and repulsive forces between the AuNRs to modulate their handedness via DNA's twist−stretch coupling. Furthermore, by elucidating how factors such as the aspect ratio of the nanorods and the length of the bridging DNA affect the free energy landscape, we show how the responsiveness of the dimers to changes in solvent conditions can be tuned from "soft" where dimers sensitively reconfigure their chirality to "rigid" where dimers maintain their chiral or achiral configuration. Our results show good agreement with experimentally observed behaviors and furthermore explain the physical basis for these behaviors. We expect that the mechanisms and principles introduced here will aid in the design of AuNR-based nanodevices with controllable chirality.

RESULTS AND DISCUSSION

Model Development. To investigate the configuration of AuNR dimers, we developed a theoretical model for calculating their free energy as a function of their internal configuration. The modeled system (Figure 1a) consists of a pair of polymer-grafted AuNRs connected by dsDNA present in a solvent medium containing ions and depletants. The internal configuration of such dimers can be described in most general terms by the surface separation distance *d* of its nanorods in the direction perpendicular to their interacting facets, the stagger of the rods in directions parallel to the interacting facets, and the relative orientation of the rods. Given that the AuNR dimers do not exhibit significant stagger in the experiments,[23] we assume that the relative positions of the AuNRs can be described completely by *d*. In addition, as the NRs are grafted with polymers of brush length comparable to the length of the bridging DNA, the interacting facets are expected to be nearly parallel. The relative orientation of AuNRs can then be described by a single twist or dihedral angle ϕ between the rods. Thus, the free energy landscape of

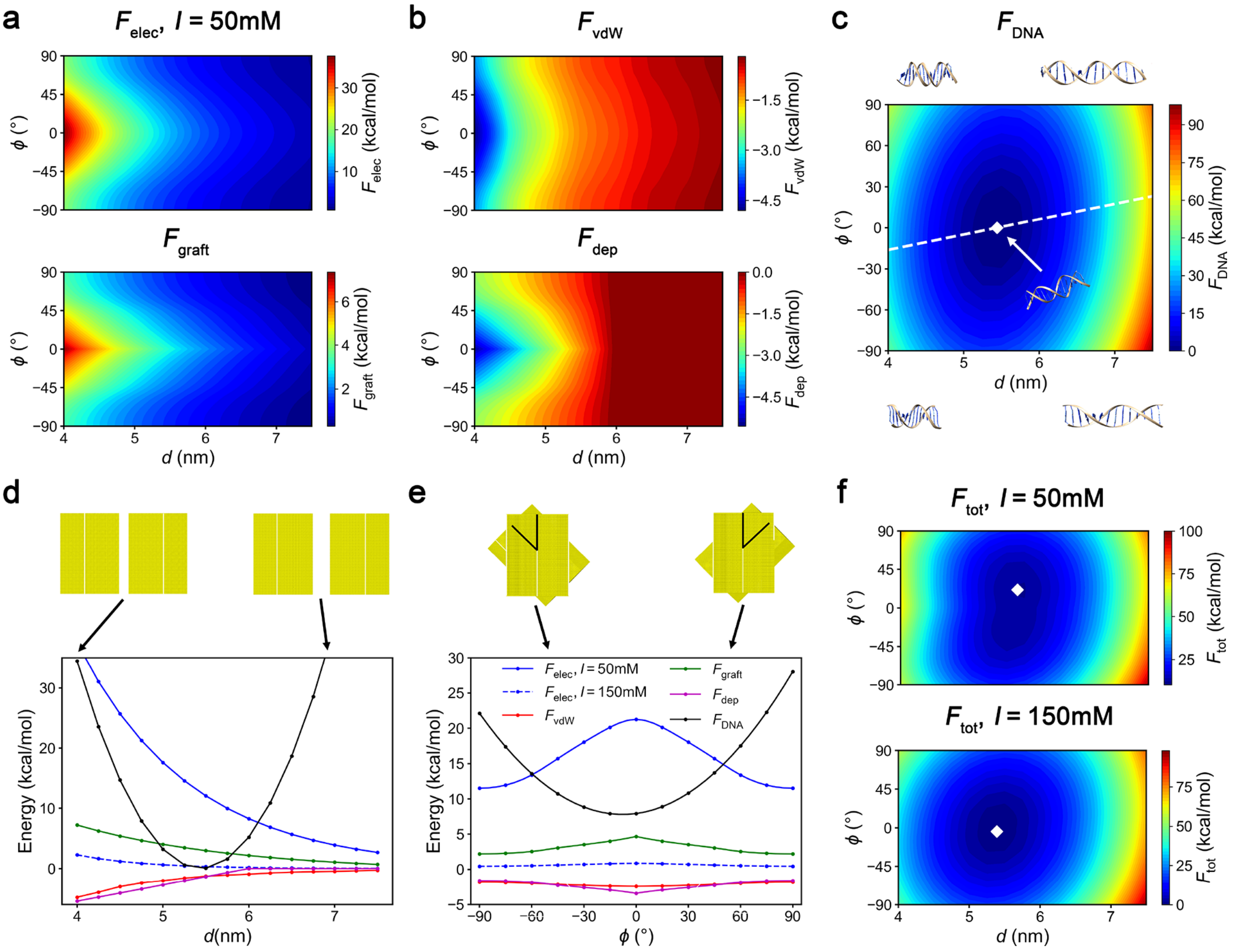

Figure 2. Free energy landscape of AuNR dimers and its contribution from various interactions. (a−c) Configuration dependence of free energy contributions from repulsive interactions F_{elec} at I = 50 mM and F_{graft} (a), attractive interactions F_{vdW} and F_{dep} (b), and dsDNA bridge F_{DNA} with $\phi_0 = 0°$ (c). The white diamond symbol specifies the dimer configuration with minimum F_{DNA}, and the dashed line marks the ϕ that yields the minimum F_{DNA} at the particular d. (d,e) Cross sections of the free energy landscape with respect to d at fixed $\phi = 0°$ (d) and ϕ at fixed d = 5 nm (e). (f) Overall free energy landscape F_{tot} at I = 50 mM (top) and I = 150 mM (bottom). White diamonds specify minimum-free-energy configurations of the dimers. All landscapes were computed using ζ = 20 mV, h_{graft} = 5 nm, c_{dep} = 300 mg/mL, AuNR aspect ratio = 1.31, and dsDNA bridge length = 15 bp.

AuNR dimers can be suitably described in terms of just two internal coordinates, d and ϕ (Figure 1b).

In our model, the overall (total) free energy (F_{tot}) of the AuNR dimer includes contributions from various different intermolecular interactions: vdW attraction between nanorods (F_{vdW}, Figure 1c), screened electrostatic interactions between ionized groups on surface of rods (F_{elec}, Figure 1c), steric interactions between grafted polymer chains (F_{graft}, Figure 1d), depletion attraction due to surrounding macromolecules (F_{dep}, Figure 1e), and stretching and twisting resistance of dsDNA (F_{DNA}, Figure 1f). Given that the overall size of the AuNR dimer system (∼50−100 nm) is beyond the capability of atomistic simulations, we used a judicious combination of theory and atomistic calculations to calculate the free energy. Specifically, to obtain F_{vdW} and F_{elec}, we computationally constructed two penta-twinned AuNRs out of a face-centered cubic lattice of gold atoms in accordance with their experimentally observed morphology (Figure 1a).[29] From this model, F_{vdW} was calculated as the summation of the Lennard-Jones (LJ) interactions acting between all pairs of atoms across the two rods. F_{elec} was also atomistically calculated, by summing the Debye−Hückel interactions between all pairs of surface atoms of the nanorods, as a function of the ionic strength (I) of the medium and the zeta potential (ζ) of the nanorods. To obtain F_{graft}, F_{dep}, and F_{DNA}, existing analytical models parametrized to match the experimental conditions were employed. In particular, the de Gennes model[30] was used to compute F_{graft} as a function of the polymer brush height (h_{graft}). F_{dep} was calculated using the Asakura−Oosawa model[31,32] as a function of depletant concentration (c_{dep}). Lastly, F_{DNA} was obtained using the elastic-rod model of DNA[28] based on the elastic constants associated with stretching (C_s) and twisting (C_t) DNA, the twist−stretch coupling coefficient (C_{ts}), and the interparticle configuration of the nanorods (d_0 and ϕ_0) at which the DNA is in its equilibrium conformation.

In this manner, the total free energy of the nanorod dimers can be expressed as a function of their configuration (d, ϕ), solvent conditions (I, c_{dep}), and material properties (rod dimensions, and lengths of polymer grafts and bridging dsDNA). The stable assembly configuration of the nanorods can then be determined by the combination of d and ϕ values that minimizes F_{tot}. Our theoretical model does not utilize the most sophisticated approaches for calculating each intermo-

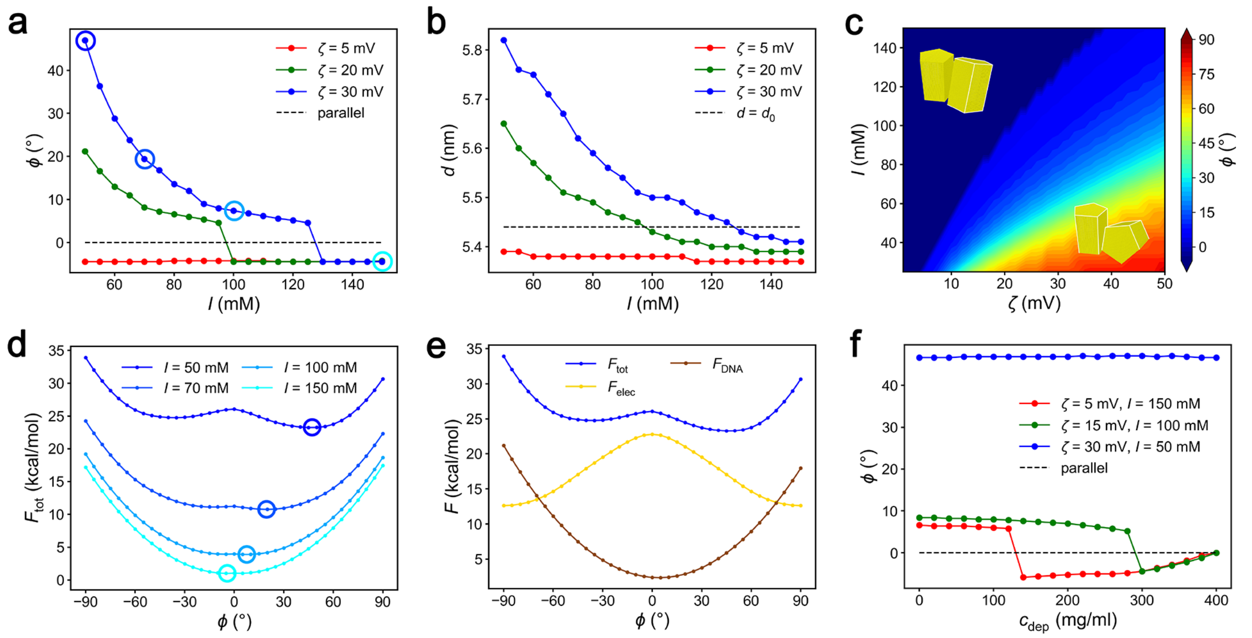

Figure 3. Solvent-mediated reconfiguration of AuNR dimers. Variation in dimer twist angle ϕ (a) and separation distance d (b) with ionic strength I for nanorods of different zeta potentials ζ. (c) Combined effect of I and ζ on ϕ. (d) ϕ-dependence of dimer free energy F_{tot} at I = 50 mM, 70 mM, 100 mM, and 150 mM for rods of ζ = 30 mV, where d = 5.82, 5.66, 5.50, and 5.41 nm at the four ionic strengths, respectively. Open circles denote the MFE ϕ. (e) Breakdown of the dimer free energy landscape plotted in blue in (d) corresponding to I = 50 mM into contributions F_{elec} and F_{DNA}. (f) Variation of ϕ with depletant concentration c_{dep}. In all plots, except (c), h_{graft} = 5 nm and c_{dep} = 300 mg/mL. The aspect ratio of the rods is 1.31 and the bridging dsDNA is 15 bp long.

lecular interaction and simplifies some molecular-level phenomena such as interactions between the DNA and the grafted polymer, and their grafting distribution and polydispersity. However, the model is physically intuitive and computational efficient, making it ideal for exploring dimer configurations for an expansive range of solvent conditions and material properties. Moreover, because all interaction potentials and parameters are experimentally derived, we expect that the model will be reasonably accurate in representing the experimentally observed behavior of AuNR dimers.

Configuration-Dependent Interaction Energies. As the overall free energy of the dimers is determined by the interplay of various interactions, it is vital to first understand how the magnitude of each individual interaction varies with dimer configuration. We begin by examining the free energy landscape contributed by each non-DNA interaction, as calculated via eqs 1−4 (Figure 2a and b). As expected, the polymer graft and electrostatic interactions are repulsive (free energy $F > 0$), whereas the vdW and depletion interactions are attractive ($F < 0$). In all cases, the interaction strength ($|F|$) rises with decreasing separation distance d and twist angle ϕ between the rods. Thus, on their own, the attractive vdW and depletion interactions would cause the rods to come close to each other ($d \to 0$) in parallel configuration ($\phi \to 0°$), which maximizes the area overlap between the interacting facets of the two rods. In contrast, the repulsive steric and electrostatic interactions would cause the rods to be perpendicular and far separated ($d \to \infty$ and $\phi \to \pm 90°$). It is important to note that none of these interactions lead to any chirality preference, as $F(\phi) = F(-\phi)$. We also note that the strength of some of these interactions is sensitive to solvent conditions. For example, compare F_{elec} at I = 50 mM and I = 150 mM in Figure 2d and e. F_{elec} is the strongest interaction and displays the largest variation with changing d and ϕ at I = 50 mM, but the same interaction becomes the weakest and the least variable with respect to dimer configurations at I = 150 mM, where electrostatic repulsion becomes more strongly screened by the ions. Therefore, we can expect that the force(s) that dominate the AuNR interactions, and thereby its stable configuration, would depend on solvent conditions.

We next examined the elastic free energy of the bridging DNA calculated using eq 5 (Figure 2c). The results show strong parabolic energy penalties to twisting, stretching, and compressing DNA relative to its equilibrium configuration (d_0 and ϕ_0), as marked by the white diamond in the figure. The mechanical resistance of DNA thus acts as a mediating force between the attractive and repulsive non-DNA interactions. While non-DNA interactions clearly steer the dimers toward $d \to \infty$ and $\phi \to \pm 90°$ or $d \to 0$ and $\phi \to 0°$, DNA pulls the dimers closer to its own energetically favored configuration, toward $d \to d_0$ and $\phi \to \phi_0$. Since the energetic penalty of deforming DNA is large and dominates the rest of the interactions (see Figure 2d and e), the dimers have to assemble close to the DNA's equilibrium configuration. We also observe that the twist−stretch coupling of dsDNA causes the free energy landscape to become "tilted" about d_0 and ϕ_0. In particular, the twist angle that yields the minimum elastic free energy for fixed d is not constrained to ϕ_0 but varies linearly with d as indicated by the white dashed line. We will denote this angle by $\phi_{min}(d)$, and its value can be obtained by setting $\frac{\partial F_{DNA}}{\partial \phi}\Big|_d = 0$ in eq 5 to yield $\phi_{min} = \phi_0 - \frac{C_{ts}}{C_t}(d - d_0)$ (note that $C_{ts} < 0$). Thus, the twist−stretch coupling effect causes the DNA to twist in the negative direction relative to ϕ_0 when it is compressed from its equilibrium length ($d < d_0$) and in the positive direction when DNA is stretched ($d > d_0$). The asymmetry in the F_{DNA} landscape also means that $F(\phi) \neq$

$F(-\phi)$ (for all $d \neq d_0$), implying that F_{DNA} is the only interaction component to display chirality preference and must therefore be responsible for the experimentally observed chirality of DNA-bridged AuNR dimers.

Together, these DNA and non-DNA interactions could lead to an interesting behavior wherein a AuNR dimer adopts left- or right-handed chiral configurations depending on the type of interaction (repulsive or attractive) dominating the non-DNA portion of the overall free energy. Consider a system dominated by *repulsive* non-DNA interactions, such as dimers present in a low-salt medium with I = 50 mM where F_{elec} is large (solid blue lines in Figure 2d and e). The net force acting on the rods due to non-DNA interactions is then repulsive, so the DNA should stretch beyond its equilibrium length. This would cause the minimum free energy (MFE) configuration of the dimer to extend beyond its "equilibrium" distance ($d > d_0$), resulting in a positive change in its twist angle ($\phi > \phi_0$) based on the twist−stretch coupling effect discussed above. Indeed, we observe that the MFE configuration shifts toward a more extended and positively twisted (right-handed chiral) state in the overall free energy landscape obtained at I = 50 mM (Figure 2f, top). Now, consider this same dimer system in a high-salt medium with I = 150 mM, where F_{elec} is much smaller (dashed blue lines in Figure 2d and e) and *attractive* non-DNA interactions dominate. Now the DNA would become compressed and the MFE configuration contracts ($d < d_0$), which should result in a negative change in the twist angle ($\phi < \phi_0$), leading to negatively twisted (left-handed chiral) dimers, as observed in the overall free energy landscape calculated at I = 150 mM (Figure 2f, bottom).

Solvent-Dependence of Dimer Configurations. The above example showing changes in dimer chirality with salt concentration highlights the crucial role played by the solvent in determining dimer configurations. To investigate this further, we used our model to determine the MFE configuration of the DNA-bridged AuNR dimers as a function of ion concentration (I) and depletant concentration (c_{dep}). The effects of I on dimer twist angle ϕ and separation distance d are shown in Figure 3a and b. Our results show that the response of the rods to varying I depends on their surface charge density. For moderately to strongly charged rods with zeta potentials of ζ = 20 mV and 30 mV, the dimers undergo switches in chirality as ionic strength is changed. At low I, the nanorods assemble with large and positive ϕ and $d > d_0$ because their non-DNA interactions are dominated by electrostatic repulsion F_{elec}. However, as I is increased, the electrostatic repulsion becomes screened, and the system becomes more attraction dominated, causing the distance between the nanorods to decrease. When d is reduced below d_0 (denoted by dashed line in Figure 3b) where DNA begins to get compressed, we observe a sharp switch in chirality from positive to negative ϕ, as shown in Figure 3a. For weakly charged nanorods with ζ = 5 mV, the dimers are insensitive to changes in I. This is because F_{elec} is weak even at low I, and changes in its magnitude are insignificant compared to the overall free energy. The combined effect of ζ and I on ϕ is presented as a contour plot in Figure 3c. This plot shows in more comprehensive manner how the dimer configuration becomes more sensitive to changes in ion concentration with increasing ζ. For instance, weakly charged rods of ζ = 5 mV exhibit small variations in twist angle in the range −4° to 6°, while strongly charged rods of ζ = 50 mV exhibit twists ranging from −4° at high I to 85° at low I. The sensitivity of AuNR dimers to surface charge density and solvent ionic strength should make them useful as chiroptical sensors for detecting changes in solvent environments.

To elucidate the energetic basis of the "chirality switching" behavior observed in Figure 3a, we examined the free energy F_{tot} of the ζ = 30 mV dimers as a function of ϕ at various fixed values of I while holding d fixed at the value corresponding to the MFE configuration at the given I (Figure 3d). For the F_{elec}-dominated case of I = 50 mM, we observe an energy barrier at $\phi \approx 0°$ separating two energy minima located at $\phi \approx -36°$ and $\phi \approx 47°$ with the latter minimum being deeper and thereby determining the positively twisted MFE configuration. This ϕ-dependence of F_{tot} may be understood by examining its components plotted in Figure 3e; only F_{elec} and F_{DNA} are shown as the magnitudes of the other components are negligible. We find that F_{elec} repulsion is strongest at ϕ = 0° and slowly decays as $|\phi|$ increases, while F_{DNA} rises parabolically about $\phi_{min} \approx 5°$ (>0° due to twist−stretch coupling). The two minima in F_{tot} arise due to the combination of a slowly decreasing $|\partial F_{elec}/\partial\phi|$ and linearly increasing $|\partial F_{DNA}/\partial\phi|$ with increasing $|\phi|$, which ensures the existence of a positive and negative ϕ where the stability condition $\partial F_{elec}/\partial\phi = -\partial F_{DNA}/\partial\phi$ is satisfied. In addition, as $d > d_0$ in this repulsion-dominated system, the energetic penalty for twisting DNA to arbitrary $\pm\phi$ angles is greater in the negative than the positive direction, as $\phi_{min} > 0°$. Therefore, the positively twisted state is energetically more favorable at I = 50 mM. However, as I is increased, $|F_{elec}|$ decreases, while F_{DNA} remains the same. Therefore, the ratio of $|\partial F_{elec}/\partial\phi|$ to $|\partial F_{DNA}/\partial\phi|$ is reduced, and the dimers exhibit smaller ϕ at their MFE configuration. When F_{elec} is further reduced, d decreases below d_0, and ϕ_{min} < 0°, the energy minimum at negative ϕ becomes slighly more favorable compared to that at positive ϕ, as observed in the F_{tot} plotted for I = 150 mM in Figure 3d.

Next, we studied the effect of c_{dep} as shown in Figure 3f. As we observed with changing I, the response of the dimers to changes in c_{dep} also depends on the balance of interactions. For example, when I = 50 mM and ζ = 30 mV, the dimers are unresponsive to changes in c_{dep}, as F_{elec} dominates the system. However, when F_{elec} becomes weaker, the dimers undergo a transition from $\phi > 0°$ to $\phi < 0°$ to $\phi \to 0°$ as c_{dep} is increased. The first transition clearly occurs due to the change in non-DNA interactions from repulsive to attractive as depletion forces become stronger, but the origin of the second transition is less obvious. To understand this transition, we must take into account the opposing effects of attractive non-DNA interactions and F_{DNA}. In the attraction-dominated regime, the DNA forces the AuNR dimers to be negatively twisted as $d < d_0$, while the non-DNA interactions drive the dimers toward the parallel configurations. Although the twist−stretch coupling effect of DNA overcomes the effects of non-DNA interactions at moderate c_{dep}, F_{dep} eventually dominates the interparticle interactions and forces the nanorods to be parallel to each other as c_{dep} is increased.

Based on these results, we can now generalize the mechanism by which these different interactions play with each other to determine the configuration of the AuNR dimers, as depicted schematically in Figure 4. For convenience, we denote the cumulative free energy from all attractive non-DNA interactions by F_{att} and that from all repulsive non-DNA interactions by F_{rep}. Depending on their relative magnitudes, the AuNR dimers will exhibit either $d < d_0$ when $|F_{att}| > |F_{rep}|$ or $d > d_0$ when $|F_{att}| < |F_{rep}|$. Therefore, as a result of twist−stretch

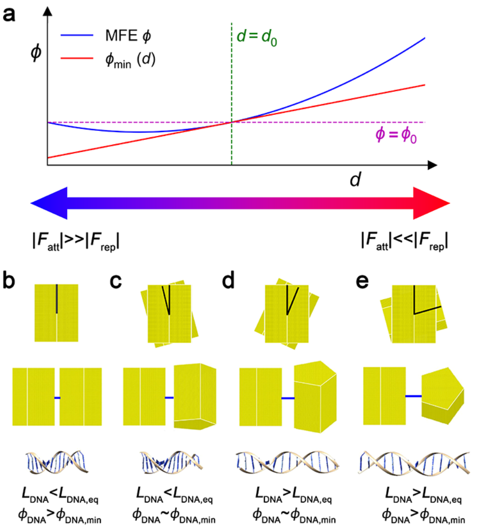

Figure 4. Overall mechanism for the observed chiral behavior of AuNR dimers: (a) Schematic relationship between d and ϕ of the dimers showing emergence of negative and positive chirality from interplay between the twist−stretch coupling of DNA and the attractive or repulsive non-DNA interactions. (b−e) Schematics showing the front and side views of the AuNR dimers and the side view of the bridging dsDNA for dimers that are strongly (b) and weakly (c) dominated by attractive interactions, and weakly (d) and strongly (e) dominated by repulsive interactions. Figures are not drawn to scale.

coupling, the DNA will try to twist the rods in the direction of positive ϕ as F_{rep} is increased and toward the negative direction as F_{att} is increased. However, the non-DNA interactions affect the rod configurations differently depending on whether the system is dominated by F_{rep} or F_{att}. As $|F_{\mathrm{rep}}|$ increases, the non-DNA interactions will try to twist the nanorods away from the parallel configuration *in concert* with DNA, causing both d and ϕ to increase monotonically. However, as $|F_{\mathrm{att}}|$ increases, the non-DNA interactions will try to reduce ϕ toward the parallel configuration *against* DNA's twist−stretch coupling effect. Therefore, while increase of $|F_{\mathrm{att}}|$ will at first lead to more negatively twisted nanorods, the rods will eventually approach the parallel configuration ($\phi = 0°$) due to the effects of F_{vdW} and F_{dep}. In summary, as the nanorods change from attraction-to repulsion-dominated regime, the configuration of the dimers will transition in the following order: parallel (strongly dominated by attractive interactions, Figure 4b), left-handed chiral (weakly dominated by attractive interactions, Figure 4c), and right-handed chiral (weakly and strongly dominated by repulsive interactions, Figure 4d and e).

Material-Dependence of Dimer Configurations. We next investigated how the material properties of the AuNR dimers impact their reconfiguration with respect to changes in I and ζ as observed in Figure 3c. We first examined the effects of changing the length of the hybridized portion of the bridging DNA. As shown in Figure 5a, the main effect of modifying DNA length is in changing the "intrinsic" separation

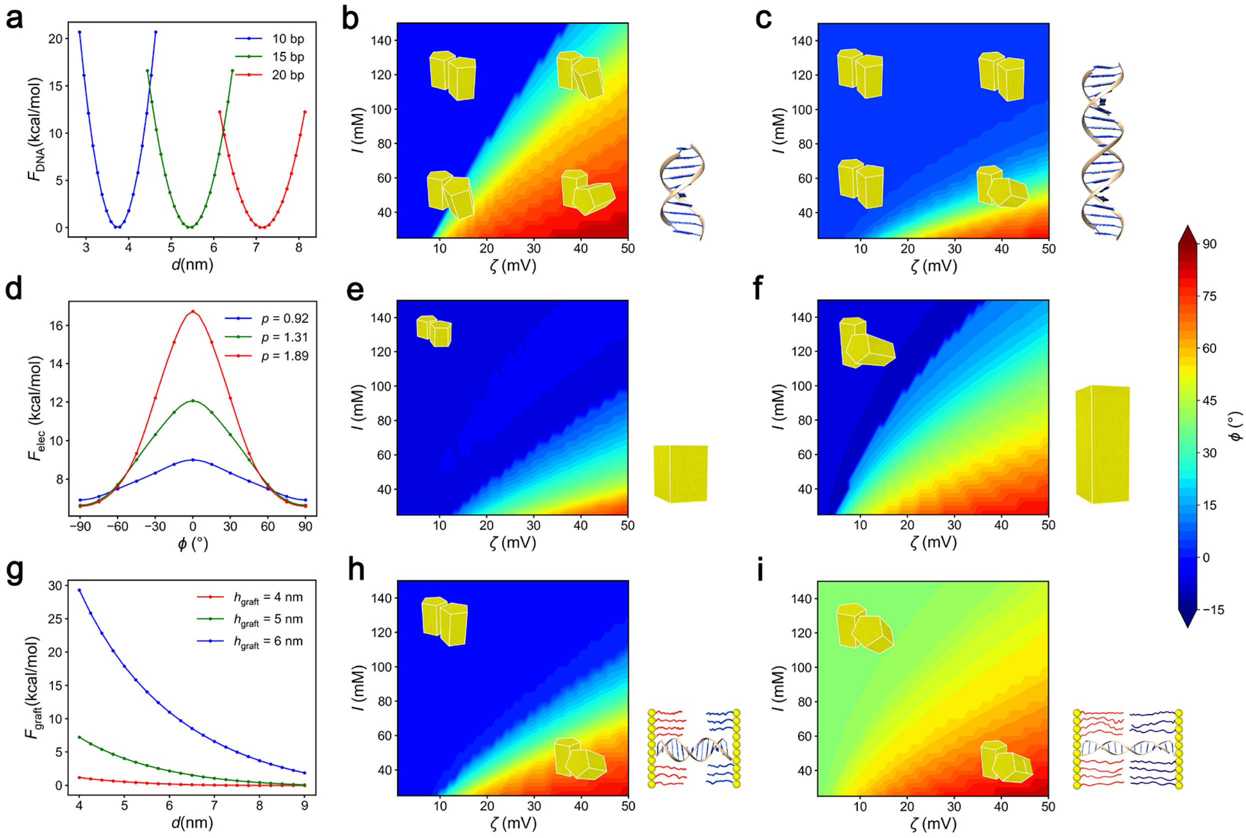

Figure 5. Material-dependent response of dimers to solvent conditions. (a) F_{DNA} as a function of d for dsDNA of different lengths. ζ- and I-dependence of ϕ for (b) 10 bp and (c) 20 bp. (d) F_{elec} as a function of ϕ for nanorods of different aspect ratios. ζ- and I-dependence of ϕ for (e) p = 0.92 and (f) p = 1.89 nanorods. (g) F_{graft} as a function of d. ζ- and I-dependence of ϕ for (h) L_{graft} = 4 nm and (i) L_{graft} = 6 nm. c_{dep} = 300 mg/mL in all cases. L_{graft} is set to 3.5 nm in (b) and to 5 nm in (c,e,f). p = 1.31 and DNA length is set equal to 15 bp in all cases unless otherwise indicated.

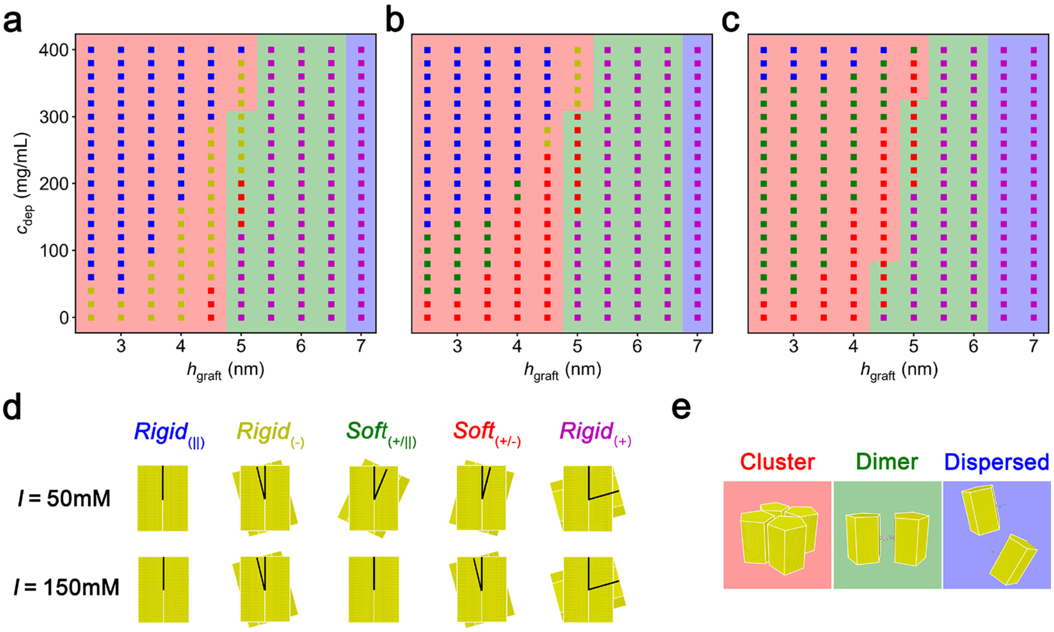

Figure 6. Response of AuNR dimers to changes in ion concentration. Responses are analyzed as a function of c_{dep} and h_{graft} for nanorods carrying different surface charges: (a) ζ = 5 mV, (b) ζ = 10 mV, (c) ζ = 20 mV. The different symbols correspond to the five classes of responses illustrated in (d), while the background shade signifies the three dispersion states of the AuNRs shown in (e). The aspect ratio of AuNR was fixed to 1.31 and the dsDNA length to 15 bp.

distance d_0 between nanorods, which increases from 3.74 nm for 10 bp DNA to 7.14 nm for 20 bp DNA. Given that all non-DNA interactions vary with d (see Figure 2d), changes in DNA length are expected to significantly affect the overall magnitudes and balance of these interactions. The effect of changing DNA length is shown in Figure 5b and c. The AuNRs bridged by 10 bp DNA display stronger variation in ϕ as compared to those with 20 bp DNA, where the AuNRs remain mostly parallel across the full range of I and ζ explored. Such behavior can again be explained by the competition between F_{elec} and F_{DNA} as depicted in Figure 3e. For AuNRs bridged by 20 bp DNA, d_0 is large and F_{elec} is accordingly quite weak. Since the small energetic gain in F_{elec} due to increase in ϕ is outweighed by the larger energetic penalty from F_{DNA} (Figure S1b), large changes in ϕ are suppressed. In contrast, the AuNRs exhibit larger changes in twist when bridged by 10 bp DNA, as the electrostatic interactions are more dominant (Figure S1a). While it may be argued that the 20 bp DNA is softer and incurs lesser energy penalty for twisting than the 10 bp DNA (see Figure 5a), the differences in the magnitudes of the non-DNA interactions far outweigh the changes in the softness of DNA with length. Therefore, the range of ϕ variations that the nanorods display with changes in solvent conditions rapidly dimimishes with increasing DNA length.

Another parameter we investigated is the AuNR aspect ratio p, defined as the ratio of its height h to its width w. The aspect ratio is an important factor, as it affects the ϕ-dependence of all non-DNA interactions. For example, F_{elec} shows much stronger variations with ϕ for large aspect-ratio rods than small ones (Figure 5d). This is because F_{elec} is roughly proportional to the interacting surface area of the two rods, and therefore F_{elec} ($\phi = \pm 90°$) $\propto w^2$, whereas F_{elec} ($\phi = 0°$) $\propto wh$ (or pw^2). To elucidate the effects of p on dimer configuration, we computed ϕ as a function of ζ and I for nanorods of aspect ratios 0.92 and 1.89 (Figure 5e and f). Our results show that rods with larger p exhibit larger variations in ϕ with respect to ζ and I, a behavior that also can be linked to the competition between F_{elec} and F_{DNA}. At small aspect ratios, F_{elec} $(\pm 90°) \simeq F_{elec}$ $(0°)$ and $|\partial F_{elec}/\partial \phi|$ is negligible (see Figure S1c). Thus, the energetic cost ΔF_{DNA} of twisting DNA outweighs the energetic benefit ΔF_{elec} from twisting the rods, which suppresses large changes in twist angle due to changing solvent conditions. However, when the p is large, $|\partial F_{elec}/\partial \phi|$ is large and becomes comparable to $|\partial F_{DNA}/\partial \phi|$ (see Figure S1d). Thus, the longer nanorods can twist more in response to changing solvent conditions as the energetic benefit ΔF_{elec} to twisting is larger. Note that while our model currently considers only penta-twinned AuNRs, these findings should be equally applicable to single-crystalline AuNRs as long as the rods are faceted.

Lastly, we investigated the effect of the length of the grafted polymers, which provide constant repulsion between the rods regardless of I or ζ (Figure 5g). We investigated dimer configurations for two different polymer brush heights h_{graft} = 4 nm ($<d_0$) and 6 nm ($>d_0$) (Figure 5h and i). Unlike the $h_{graft} < d_0$ case in which we observe a wide range of ϕ values spanning negative to positive chirality, we observe that ϕ is always larger than ~35° when $h_{graft} > d_0$. This is because the grafts are longer than the equilibrium length of the DNA, which causes $|F_{rep}|$ to always be greater than $|F_{att}|$ regardless of solvent conditions. Therefore, such situations will lead to AuNR dimers that are always right-handed chiral.

Reconfigurability. Our results so far have demonstrated that the AuNR dimers can exhibit different configurations depending on material properties and solvent conditions. To better characterize the reconfigurability of dimers, we systematically analyzed how their twist angle ϕ changes as I is increased from 50 mM to 150 mM for different combinations of c_{dep}, h_{graft}, and ζ. The response of the dimers could be broadly categorized into "soft" and "rigid" behaviors to differentiate dimers that are highly sensitive to changes in I from those that are relatively insensitive to I; the two behaviors were further divided to yield five distinct classes of behaviors as depicted in Figure 6d: (1) *Rigid*$_{(\|)}$, where nanorods remain parallel regardless of I, a behavior occurring when F_{att} remains strongly dominant over F_{rep} regardless of I (see Figure 4b); (2) *Rigid*$_{(-)}$, where dimers remain negatively twisted regardless of I, which occurs when F_{att} is slightly stronger than F_{rep} across all I; (3) *Soft*$_{(+/\|)}$, where dimers are positively twisted at I = 50 mM and parallel at I = 150 mM, which occurs when F_{elec} is dominant at low I and gets outweighed by F_{att} at high I; (4) *Soft*$_{(+/-)}$, where dimers switch their chirality as I is changed, which occurs when F_{rep} is weakly dominant at low I but F_{att} becomes dominant at high I; and (5) *Rigid*$_{(+)}$, when F_{rep} is dominant regardless of I and the dimers remain positively twisted.

Figure 6a−c shows the above responses mapped onto the parameter space of depletant concentration and polymer brush height at different values of the AuNR zeta potential. We first examine dimers with ζ = 10 mV whose responses are depicted in Figure 6b. When c_{dep} is large and h_{graft} is small, the dimers exhibit *Rigid*$_{(\|)}$ behavior, consistent with F_{att} being dominant across the entire range of I due to the strong depletion attraction F_{dep}, which overwhelms both the electrostatic repulsion F_{elec}, even at low I, and the graft−graft repulsion F_{graft} that is negligible in this region (see Figure 3b). In a small region of the parameter space where c_{dep} is large but h_{graft} is moderate, the dimers exhibit *Rigid*$_{(-)}$ behavior. Similar to the above region, $F_{\text{att}} > F_{\text{rep}}$ irrespective of I, but the attractive interactions are not as dominant because F_{graft} is not negligible anymore. Thus, the dimers prefer a slightly negatively twisted configuration to avoid the stronger graft repulsion at ϕ = 0° (see Figure 3d). A further increase in h_{graft} results in the *Rigid*$_{(+)}$ behavior, as the repulsive F_{graft} now dominates the interactions regardless of I (see Figure 3e), as is the case observed in Figure 5i. In fact, when h_{graft} > 5.5 nm, the dimers are always positively twisted regardless of I or c_{dep}.

In between the regions of *Rigid*$_{(\|)}$ and *Rigid*$_{(+)}$ behaviors, we observe dimers displaying strong sensitivity to I. When c_{dep} and h_{graft} are both small, the dimers exhibit *Soft*$_{(+/-)}$ chirality-switching behavior. Here, F_{graft} is negligible and F_{dep} is also not strong. Therefore, at low I where F_{elec} is large, F_{rep} becomes dominant leading to positively twisted dimers; at high I where F_{elec} becomes small, F_{att} becomes dominant leading to negatively twisted states. Further increase in c_{dep} results in a *Soft*$_{(+/\|)}$ response, where the dimers still exhibit positive twist at low I as above, but at high I, the attractive interactions more strongly dominate the other interactions than above, causing the nanorods to become parallel rather than negatively twisted to each other.

The locations of the soft and rigid responses in the h_{graft}−c_{dep} parameter space depends on the surface charges carried by the rods. When ζ is decreased to 5 mV as shown in Figure 6a, we observe an expansion of rigid responses and disappearance of soft responses. This is because F_{elec} becomes negligible at small ζ values, and the dimer configuration becomes less sensitive to changes in I. In contrast, when ζ is increased to 20 mV as shown in Figure 6c, soft responses become more prevalent. Here, changes in I lead to larger differences in F_{elec}, which results in increased reconfiguration of the dimers with changes in I. Table 1 provides a summary of the general effects of the material parameters described in Figures 5 and 6 on the responsiveness of AuNR dimers to solvent conditions.

We finally investigated how solvent conditions affected the stability of the dimerized state of the AuNRs. If the non-DNA interactions between nanorods are repulsive and larger in magnitude than the hybridization energy of the bridging dsDNA (predicted to be −17.5 kcal/mol through DINAMelt software[33]), we can expect the AuNRs to stay dispersed in solution. On the other hand, if the non-DNA interactions are sufficiently attractive, the AuNRs will aggregate into clusters. These three possible dispersion states of AuNRs are overlaid onto Figure 6a−c. In all cases, the AuNRs should stay dispersed when $h_{\text{graft}} \geq 7$ nm. This is expected as the long grafts will only allow the assembly of AuNRs when the DNA is greatly stretched beyond its equilibrium length, which is energetically very costly. Interestingly, a large number of *Rigid*$_{(+)}$ states remain stable in the dimer state. When $h_{\text{graft}} \leq 4$ nm, the AuNRs prefer to aggregate into clusters when I is 150 mM. This suggests that utilization of these nanoparticles in solvents with high ionic concentrations requires grafted polymers of $h_{\text{graft}} \approx d_0$ for stability.

Table 1. Qualitative Effect of Material Properties on the Responsiveness of AuNR Dimers

property	small	large
Aspect ratio (p)	Rigid	Soft
Surface charge (ζ)	Rigid	Soft
DNA length (L_{DNA})	Soft	Rigid
Graft height (h_{graft})	Soft	Rigid

Comparison with Experiments. To assess the predictive strength of our computational model, we compared its predictions to the experimentally reported configurations. However, a quantitative evaluation of the model's accuracy against experiments is difficult. First, the interparticle configuration (d and ϕ) of AuNRs is difficult to measure experimentally and is often not reported. In such cases, the chirality of the AuNRs must be inferred from their chiroptical properties such as their circular dichroism spectra. Second, the solvent conditions (I, c_{dep}, and pH) and material properties (ζ) are often unclear when the experiments use biological media. Nevertheless, many of the experimentally observed trends are explained by our model. For example, Sun et al.[22] reported that oblong gold nanoparticles (aspect ratio ∼1.3) transitioned from right- to left-handed chirality as the concentration of NaCl was increased. This transition is consistent with results from our theoretical model (Figure 3a) and stresses the role of electrostatic interactions in dictating dimer chirality. In addition, this study observed that the nanoparticles change their twist angles from $\phi \approx 6°$ in solutions containing bovine serum albumin (BSA) at concentrations of 200 mg/mL to $\phi \approx -6°$ for solutions with BSA concentration of 400 mg/mL. While our model does not consider BSA specifically as the depletant, the observed effect of depletants on dimer configurations agrees not only qualitatively but also almost quantitatively with our predictions at ζ = 20 mV in Figure 3f.

Furthermore, multiple experiments have observed that the AuNR dimers reconfigure from positive to negative chirality, as they transition from extracellular (cell culture medium) to intracellular environments.[20,22] This difference in configuration can be attributed to the different concentrations of macromolecules and salt in the two media. The intracellular environment generally contains high concentrations of macromolecules (such as proteins) in the range of 200 to 400 mg/mL,[34−36] while the extracellular environment contained considerably smaller amount of proteins (<50 mg/mL). The ionic strength of the intracellular environment was also high (I > 150 mM)[37,38] compared to the extracellular medium where positive chirality was observed ($I < 50$ mM).[22] Consequently, the nanorods are dominated by attractive interactions in the intracellular environment—as high I and c_{dep} lead to weak F_{elec} and strong F_{dep}—while repulsive interactions are expected to dominate in the extracellular medium. Our theoretical model that relates the chirality of AuNRs to the balance between attractive and repulsive interactions (Figure 4) indeed explains and predicts (see Figure S2) such experimentally observed chirality switches.

Finally, experiments[20,22] have revealed that AuNRs functionalized with CTAB transition from the dimerized state in the extracellular environment to aggregated clusters in the intracellular environment. The dispersion stability of CTAB at low I arises from the electrostatic interactions between charges on CTAB; however, in high I environments, this repulsion is strongly screened, and the steric hindrance between the CTAB molecules, which are quite short, is not sufficient to prevent aggregation of the AuNRs. Our computational results indeed demonstrate that regardless of ζ, the nanorods will aggregate into clusters in high I medium if $h_{\mathrm{graft}} <$ 4 nm (Figure 6a−c). Also in agreement with our predictions, the experiments have shown that grafting the same AuNRs with longer poly(styrene-*b*-acrylic acid) chains allows them to remain as stable dimers inside intracellular environments. Thus, again, our model shows good agreement with experiments and furthermore helps explain the observed behaviors in physical terms.

CONCLUSIONS

We have examined the underlying physics governing the assembly of dsDNA-bridged AuNR dimers and provided guidelines for controlling their configuration, especially their chirality. By theoretically modeling the free energy of the dimers, we demonstrated how their configuration is dictated by an interplay between the twist−stretch coupling of DNA and the intermolecular forces acting between the AuNRs. In particular, we showed that the dimers exhibit negatively twisted or parallel configurations when the free energy contribution from non-DNA interaction is dominated by attractive depletion or vdW forces and positively twisted configurations when the system is dominated by repulsive electrostatic or steric forces.

Through extensive analyses, we revealed the full range of configurations exhibited by the dimers as a function of their material properties and solvent conditions. We found that dimers can reconfigure their twist angle based on changes in ion or depletant concentration and showed how this reconfigurability can be engineered to be strongly or weakly responsive to changes in solvent conditions by tuning the height of the polymer brush, the aspect ratio of the AuNRs, or the length of the dsDNA bridge. While many of these predictions show good agreement with experimental observations, not all of the findings have been validated experimentally. For instance, the effects of nanorod aspect ratio and DNA length have not been verified through experiments. Further experimental investigations into these untested outcomes of our model would be a valuable endeavor to pursue in the future.

Understanding the relationship between material properties of the dimers and their reconfigurability is crucial for fabricating application-specific nanostructures. For example, nanosensing may require the dimers to sensitively alter their interparticle configuration in response to changes in the solvent, so that such changing solvent conditions are easily detected from the circular dichroism spectra of the nanorods. For these cases, our results suggest that using nanorods with large aspect ratios and high surface charge densities may be beneficial. However, for applications such as chiral catalysis, a rigid interparticle configuration is likely desired. For such applications, AuNRs with small aspect ratio, long grafted polymers, or low surface charge densities would be advantageous. Thus, the theoretical model developed here could be used as a guiding principle for designing chiral nanostructures with tunable properties for a variety of applications.

METHODS

The nanorods investigated in this study had a fixed width of 24 nm and heights ranging from 22 to 46 nm to match the experimentally utilized nanorods.[19,22,23] The computationally constructed atomistic model of the nanorods, as depicted in Figure 1a, was used for computing the vdW interaction free energy F_{vdW}. This involved summing up the LJ interactions acting between all pairs of atoms of the two rods as given by[39]

$$F_{\mathrm{vdW}} = \sum_{i=1}^{N}\sum_{j=1}^{N} 4\varepsilon_{\mathrm{Au}}\left[\left(\frac{\sigma_{\mathrm{Au}}}{r_{ij}}\right)^{12} - \left(\frac{\sigma_{\mathrm{Au}}}{r_{ij}}\right)^{6}\right] \tag{1}$$

Here, N, r_{ij}, $\varepsilon_{\mathrm{Au}}$, and σ_{Au} denote the number of gold atoms in each nanorod, the interatomic distance between gold atoms, and their LJ energy and size parameters, respectively (Figure 1c). σ_{Au} was set equal to 0.292 nm,[40] and $\varepsilon_{\mathrm{Au}}$ of 0.4223 kcal/mol was determined from the Hamaker constant A of gold in water (2.5×10^{-19} J)[41] and the number density ρ of the gold atoms (0.098 mol/cm^3) according to $\varepsilon_{\mathrm{Au}} = \frac{A}{4\pi^2\rho^2\sigma_{\mathrm{Au}}^6}$.[42]

The atomistic model of AuNRs was also used for obtaining the electrostatic energy F_{elec}. The rod surface is usually charged due to the presence of strongly adsorbed capping agents that often get ionized in solution (Figure 1c). Given that the coating thickness of these capping agents is generally quite small (∼0.38−0.7 nm for citrates[43] and ∼1 nm for cetyl-trimethylammonium bromide or CTAB[44,45]), we assume for convenience that the location of these surface charges coincide with the positions of the surface gold atoms in our atomically represented AuNRs. These charges on separate rods are expected to interact with each other *via* screened electrostatic interactions due to the presence of counterions and salt in the solvent medium. Accordingly, the electrostatic interaction energy between dimer rods was obtained by summing the Debye−Hückel interactions between all pairs of surface atoms across the two rods:

$$F_{\mathrm{elec}} = \sum_{i=1}^{N_{\mathrm{surf}}}\sum_{j=1}^{N_{\mathrm{surf}}} \frac{q^2}{4\pi\varepsilon r_{ij}} \mathrm{e}^{-r_{ij}/\lambda_{\mathrm{D}}} \tag{2}$$

where N_{surf}, q, ε, and λ_{D} represent the total number of surface atoms in each rod, the "effective" charge assigned to each such atom, the permittivity of water, and the Debye length. As the electrostatic interactions can become long-ranged at low salt conditions, N_{surf} includes not only the surface atoms on the facets in proximity but also the entire surface of the nanorods. The Debye length was calculated using $\lambda_{\mathrm{D}} = \sqrt{\frac{\varepsilon k_{\mathrm{B}}T}{2 \times 10^3 N_{\mathrm{A}} e^2 I}}$, where N_{A}, e, and I denote the Avogadro number, elementary charge, and ionic strength of the medium. q was obtained from the surface charge density σ_{c} and the surface area A_{surf} of the rods *via* $q = \sigma_{\mathrm{c}} A_{\mathrm{surf}}/N_{\mathrm{surf}}$, where σ_{c} was estimated from the zeta potential ζ using $\sigma_{\mathrm{c}} = 2\varepsilon k_{\mathrm{B}}T/\left(e\lambda_{\mathrm{D}}\sinh\frac{e\zeta}{2k_{\mathrm{B}}T}\right)$.[22]

AuNRs are commonly grafted with polymers such as polyethylene glycol (PEG) to prevent aggregation.[19,22,23] To describe the entropic repulsion F_{graft} from the steric hindrance of this polymer brush in good solvent, we employed the de Gennes model,[30] which has been shown to accurately reproduce the experimentally measured compression isotherms of PEG.[46,47] According to this model, F_{graft} is given by

$$F_{\mathrm{graft}} = \frac{C_1 A_{\mathrm{int}}}{2\pi}\left[7\left(\frac{d}{2h_{\mathrm{graft}}}\right)^{-5/4} + 5\left(\frac{d}{2h_{\mathrm{graft}}}\right)^{7/4} - 12\right] \quad (3)$$

Here, C_1 represents an energy constant, A_{int} the interacting surface area, d the surface separation distance between interacting facets, and h_{graft} the brush height (Figure 1d). A_{int} was calculated as the projected overlap area of the two interacting facets. C_1 is given by $\frac{16\pi h_{\mathrm{graft}}\Gamma^{1.5}}{35}k_BT$ where Γ is the grafting density of the polymer and $h_{\mathrm{graft}} = \Gamma^{1/3}R_F^{5/3}$. The Flory radius R_F is set equal to $a_{\mathrm{PEG}}N_{\mathrm{PEG}}^{0.6}$ with a_{PEG} and N_{PEG} representing the Kuhn length and number of monomers per chain of PEG. We used $a_{\mathrm{PEG}} = 0.35$ nm and $N_{\mathrm{PEG}} = 114$ to match the experimentally utilized PEG grafts of $M_w = 5000$ g/mol.[22]

Many potential applications of AuNR dimers are in biological environments, so the rods could also experience attractive depletion forces due to the presence of proteins and other macromolecules in biological media. The free energy F_{dep} associated with depletion forces was estimated using the Asakura−Oosawa formalism:[31,32]

$$F_{\mathrm{dep}} = -\Pi\Delta V_{\mathrm{exc}} \quad (4)$$

where Π is the osmotic pressure of the depletants in the solvent and ΔV_{exc} is the extra volume that becomes available to the depletants as a result of the overlap between excluded volumes of the rods at close proximity (Figure 1e). ΔV_{exc} is equal to $A_{\mathrm{interact}}(\sigma_{\mathrm{dep}} - d)$ when the surface separation distance d between the rods is smaller than the diameter σ_{dep} of the depletant, and 0 when $d > \sigma_{\mathrm{dep}}$. For convenience, we treated all depletant molecules as hemoglobin, as its osmotic pressure has been modeled previously, using $\Pi = N_A k_B T(c + 4vc^2 + 10v^2c^3 + 18.36v^3c^4 + 28.24v^4c^5 + 39.5v^5c^6 + 56.4v^6c^7)$.[48−50] Here, v and c are the molar volume and the concentration of the depletant. The diameter of the depletant was taken to be $\sigma_{\mathrm{dep}} = 6$ nm, consistent with the size of hemoglobin.

Lastly, the bridging DNA consists of dsDNA of length L_{DNA} flanked on both sides by single-stranded DNA (ssDNA) that is capped by a thiol group (Figure 1f). In experiments, the thiol group is covalently bonded to the gold surface and the ssDNA ends are strongly adsorbed onto the gold surface.[51−53] For calculating the free energy F_{DNA} associated with such DNA, we assume that the ssDNA portions as well as the terminal bases of dsDNA are fixed rigidly to the gold surface and therefore cannot rotate. The only contribution to F_{DNA} must then arise from the mechanical resistance of dsDNA, which can be treated reasonably accurately using an elastic-rod model of DNA:[28]

$$F_{\mathrm{DNA}} = \frac{C_s}{2L_{\mathrm{DNA,eq}}}(d - d_0)^2 + \frac{C_t}{2L_{\mathrm{DNA,eq}}}(\phi - \phi_0)^2 + \frac{C_{ts}}{L_{\mathrm{DNA,eq}}}(\phi - \phi_0)(d - d_0) \quad (5)$$

where C_s and C_t are the elastic constants associated with stretching and twisting of dsDNA, and C_{ts} is its twist−stretch coupling coefficient. The values of C_s, C_t, and C_{ts} were set equal to 1100 pN, 460 pN nm^2, and −90 pN nm, as measured from magnetic tweezer experiments.[28] $L_{\mathrm{DNA,eq}}$ represents the equilibrium length of dsDNA, where we assume that it is present in its natural B-form. d_0 is the surface separation distance between the interacting facets of the rods at which the length of the DNA is equal to its equilibrium value. Based on the described geometry (Figure 1f), $d_0 = L_{\mathrm{DNA,eq}} + 2L_{\mathrm{anchor}}$, where L_{anchor} is the thickness of the adsorbed layer of ssDNA assumed to be equal to 0.34 nm, the length of one base pair, in accordance with scanning tunneling microscopy measurements and molecular dynamics simulations.[53] ϕ_0 represents the twist angle of the rods that minimizes the free energy of the dimers *during* their assembly involving DNA hybridization. Experimentally, the assembly of AuNR dimers is carried out in solvents containing high concentrations of macromolecules and ions.[21] For our calculations, we assumed that assembly occurred at $I = 250$ mM ($\equiv I_0$) and $c_{\mathrm{dep}} = 400$ mg/mL ($\equiv c_0$) and that DNA hybridizes at its equilibrium length $L_{\mathrm{DNA,eq}}$. We then obtained ϕ_0 by searching for the value of ϕ that minimized $F_{\mathrm{tot}}(d = d_0, I = I_0, c_{\mathrm{dep}} = c_0)$. Thus, in effect, the above model describes the free energy of the dsDNA bridge relative to its free energy in the "equilibrium" configuration during hybridization.

ASSOCIATED CONTENT

Supporting Information

The Supporting Information is available free of charge at https://pubs.acs.org/doi/10.1021/acsnano.1c04326.

> Effect of DNA length and aspect ratio on the relative contributions of electrostatic repulsion and DNA mechanics to the overall free energy of AuNR dimers. Dimer twist angle as a function of ionic strength in intra- and extracellular environments. (PDF)

AUTHOR INFORMATION

Corresponding Author

Gaurav Arya − *Department of Mechanical Engineering and Materials Science, Duke University, Durham, North Carolina 27708, United States; Department of Biomedical Engineering, Duke University, Durham, North Carolina 27708, United States; Department of Chemistry, Duke University, Durham, North Carolina 27708, United States;* orcid.org/0000-0002-5615-0521; Phone: +1 (919) 660-5435; Email: gaurav.arya@duke.edu; Fax: +1 (919) 660-8963

Authors

Brian Hyun-jong Lee − *Department of Mechanical Engineering and Materials Science, Duke University, Durham, North Carolina 27708, United States*

Nicholas A. Kotov − *Department of Chemical Engineering, University of Michigan, Ann Arbor, Michigan 48109, United States;* orcid.org/0000-0002-6864-5804

Complete contact information is available at: https://pubs.acs.org/10.1021/acsnano.1c04326

Notes

The authors declare no competing financial interest.

ACKNOWLEDGMENTS

B.H.L. and G.A. thank the National Science Foundation (Grant CMMI 1636356) and the UC San Diego Materials Research Science and Engineering Center (UCSD MRSEC) supported by the National Science Foundation (Grant DMR-2011924) for supporting this work. N.A.K. is grateful for support of this work by the Vannevar Bush DoD Fellowship (ONR N000141812876) and the ONR COVID-19 Newton Award (HQ00342010033) for supporting the work. Computational resources were provided by the Duke Computing Cluster (DCC) and the Extreme Science and Engineering Discovery Environment (XSEDE) Program supported by the National Science Foundation (Grant ACI-1053575).

REFERENCES

(1) Hendry, E.; Carpy, T.; Johnston, J.; Popland, M.; Mikhaylovskiy, R.; Lapthorn, A.; Kelly, S.; Barron, L.; Gadegaard, N.; Kadodwala, M. Ultrasensitive Detection and Characterization of Biomolecules Using Superchiral Fields. *Nat. Nanotechnol.* **2010**, *5*, 783−787.

(2) Zhao, Y.; Xu, L.; Ma, W.; Wang, L.; Kuang, H.; Xu, C.; Kotov, N. A. Shell-Engineered Chiroplasmonic Assemblies of Nanoparticles for Zeptomolar DNA Detection. *Nano Lett.* **2014**, *14*, 3908−3913.

(3) Mori, K.; Kondo, Y.; Yamashita, H. Synthesis and Characterization of FePd Magnetic Nanoparticles Modified with Chiral BINAP Ligand as a Recoverable Catalyst Vehicle for the Asymmetric Coupling Reaction. *Phys. Chem. Chem. Phys.* **2009**, *11*, 8949−8954.

(4) Hu, A.; Yee, G. T.; Lin, W. Magnetically Recoverable Chiral Catalysts Immobilized on Magnetite Nanoparticles for Asymmetric Hydrogenation of Aromatic Ketones. *J. Am. Chem. Soc.* **2005**, *127*, 12486−12487.

(5) Jiang, S.; Chekini, M.; Qu, Z.-B.; Wang, Y.; Yeltik, A.; Liu, Y.; Kotlyar, A.; Zhang, T.; Li, B.; Demir, H. V.; Kotov, N. A. Chiral Ceramic Nanoparticles and Peptide Catalysis. *J. Am. Chem. Soc.* **2017**, *139*, 13701−13712.

(6) Li, S.; Liu, J.; Ramesar, N. S.; Heinz, H.; Xu, L.; Xu, C.; Kotov, N. A. Single-and Multi-Component Chiral Supraparticles as Modular Enantioselective Catalysts. *Nat. Commun.* **2019**, *10*, 1−10.

(7) Qu, A.; Sun, M.; Kim, J.-Y.; Xu, L.; Hao, C.; Ma, W.; Wu, X.; Liu, X.; Kuang, H.; Kotov, N. A.; Xu, C. Stimulation of Neural Stem Cell Differentiation by Circularly Polarized Light Transduced by Chiral Nanoassemblies. *Nat. Biomed. Eng.* **2021**, *5*, 103−113.

(8) Kumar, J.; Eraña, H.; López-Martínez, E.; Claes, N.; Martín, V. F.; Solís, D. M.; Bals, S.; Cortajarena, A. L.; Castilla, J.; Liz-Marzán, L. M. Detection of Amyloid Fibrils in Parkinson's Disease Using Plasmonic Chirality. *Proc. Natl. Acad. Sci. U. S. A.* **2018**, *115*, 3225−3230.

(9) Kuzyk, A.; Jungmann, R.; Acuna, G. P.; Liu, N. DNA Origami Route for Nanophotonics. *ACS Photonics* **2018**, *5*, 1151−1163.

(10) Zhou, C.; Duan, X.; Liu, N. A Plasmonic Nanorod That Walks on DNA Origami. *Nat. Commun.* **2015**, *6*, 1−6.

(11) Yeom, B.; Zhang, H.; Zhang, H.; Park, J. I.; Kim, K.; Govorov, A. O.; Kotov, N. A. Chiral Plasmonic Nanostructures on Achiral Nanopillars. *Nano Lett.* **2013**, *13*, 5277−5283.

(12) Zhou, J.; Dong, J.; Wang, B.; Koschny, T.; Kafesaki, M.; Soukoulis, C. M. Negative Refractive Index Due to Chirality. *Phys. Rev. B: Condens. Matter Mater. Phys.* **2009**, *79*, 121104.

(13) Yu, R.; Liz-Marzan, L. M.; Garcia de Abajo, F. J. Universal Analytical Modeling of Plasmonic Nanoparticles. *Chem. Soc. Rev.* **2017**, *46*, 6710−6724.

(14) Huang, X.; El-Sayed, I. H.; Qian, W.; El-Sayed, M. A. Cancer Cell Imaging and Photothermal Therapy in the Near-Infrared Region by Using Gold Nanorods. *J. Am. Chem. Soc.* **2006**, *128*, 2115−2120.

(15) Cheng, G.; Xu, D.; Lu, Z.; Liu, K. Chiral Self-Assembly of Nanoparticles Induced by Polymers Synthesized via Reversible Addition-Fragmentation Chain Transfer Polymerization. *ACS Nano* **2019**, *13*, 1479−1489.

(16) Zhang, Q.; Hernandez, T.; Smith, K. W.; Jebeli, S. A. H.; Dai, A. X.; Warning, L.; Baiyasi, R.; McCarthy, L. A.; Guo, H.; Chen, D.-H.; Dionne, J. A.; Landes, C. F.; Link, S. Unraveling the Origin of Chirality from Plasmonic Nanoparticle-Protein Complexes. *Science* **2019**, *365*, 1475−1478.

(17) Shinmori, H.; Mochizuki, C. Strong Chiroptical Activity from Achiral Gold Nanorods Assembled with Proteins. *Chem. Commun.* **2017**, *53*, 6569−6572.

(18) Zhu, Y.; Xu, L.; Ma, W.; Xu, Z.; Kuang, H.; Wang, L.; Xu, C. A One-Step Homogeneous Plasmonic Circular Dichroism Detection of Aqueous Mercury Ions Using Nucleic Acid Functionalized Gold Nanorods. *Chem. Commun.* **2012**, *48*, 11889−11891.

(19) Ma, W.; Kuang, H.; Xu, L.; Ding, L.; Xu, C.; Wang, L.; Kotov, N. A. Attomolar DNA Detection with Chiral Nanorod Assemblies. *Nat. Commun.* **2013**, *4*, 1−8.

(20) Xu, L.; Gao, Y.; Kuang, H.; Liz-Marzán, L. M.; Xu, C. MicroRNA-Directed Intracellular Self-Assembly of Chiral Nanorod Dimers. *Angew. Chem., Int. Ed.* **2018**, *57*, 10544−10548.

(21) Tang, L.; Li, S.; Xu, L.; Ma, W.; Kuang, H.; Wang, L.; Xu, C. Chirality-Based Au-Ag Nanorod Dimers Sensor for Ultrasensitive PSA Detection. *ACS Appl. Mater. Interfaces* **2015**, *7*, 12708−12712.

(22) Sun, M.; Xu, L.; Bahng, J. H.; Kuang, H.; Alben, S.; Kotov, N. A.; Xu, C. Intracellular Localization of Nanoparticle Dimers by Chirality Reversal. *Nat. Commun.* **2017**, *8*, 1−10.

(23) Ma, W.; Kuang, H.; Wang, L.; Xu, L.; Chang, W.-S.; Zhang, H.; Sun, M.; Zhu, Y.; Zhao, Y.; Liu, L.; Xu, C.; Link, S.; Kotov, N. A. Chiral Plasmonics of Self-Assembled Nanorod Dimers. *Sci. Rep.* **2013**, *3*, 1934.

(24) Shen, C.; Lan, X.; Lu, X.; Ni, W.; Wang, Q. Tuning the Structural Asymmetries of Three-Dimensional Gold Nanorod Assemblies. *Chem. Commun.* **2015**, *51*, 13627−13629.

(25) Jiang, Q.; Liu, Q.; Shi, Y.; Wang, Z.-G.; Zhan, P.; Liu, J.; Liu, C.; Wang, H.; Shi, X.; Zhang, L.; Sun, J.; Ding, B.; Liu, M. Stimulus-Responsive Plasmonic Chiral Signals of Gold Nanorods Organized on DNA Origami. *Nano Lett.* **2017**, *17*, 7125−7130.

(26) Nguyen, L.; Dass, M.; Ober, M. F.; Besteiro, L. V.; Wang, Z. M.; Nickel, B.; Govorov, A. O.; Liedl, T.; Heuer-Jungemann, A. Chiral Assembly of Gold-Silver Core-Shell Plasmonic Nanorods on DNA Origami with Strong Optical Activity. *ACS Nano* **2020**, *14*, 7454−7461.

(27) Lan, X.; Su, Z.; Zhou, Y.; Meyer, T.; Ke, Y.; Wang, Q.; Chiu, W.; Liu, N.; Zou, S.; Yan, H.; Liu, Y. Programmable Supra-Assembly of a DNA Surface Adapter for Tunable Chiral Directional Self-Assembly of Gold Nanorods. *Angew. Chem.* **2017**, *129*, 14824−14828.

(28) Gore, J.; Bryant, Z.; Nöllmann, M.; Le, M. U.; Cozzarelli, N. R.; Bustamante, C. DNA Overwinds When Stretched. *Nature* **2006**, *442*, 836−839.

(29) Lofton, C.; Sigmund, W. Mechanisms Controlling Crystal Habits of Gold and Silver Colloids. *Adv. Funct. Mater.* **2005**, *15*, 1197−1208.

(30) De Gennes, P. Polymers at an Interface: A Simplified View. *Adv. Colloid Interface Sci.* **1987**, *27*, 189−209.

(31) Asakura, S.; Oosawa, F. On Interaction between Two Bodies Immersed in a Solution of Macromolecules. *J. Chem. Phys.* **1954**, *22*, 1255−1256.

(32) Asakura, S.; Oosawa, F. Interaction between Particles Suspended in Solutions of Macromolecules. *J. Polym. Sci.* **1958**, *33*, 183−192.

(33) Markham, N. R.; Zuker, M. DINAMelt Web Server for Nucleic Acid Melting Prediction. *Nucleic Acids Res.* **2005**, *33*, W577−W581.

(34) Fulton, A. B. How Crowded Is the Cytoplasm? *Cell* **1982**, *30*, 345−347.

(35) Zimmerman, S. B.; Trach, S. O. Estimation of Macromolecule Concentrations and Excluded Volume Effects for the Cytoplasm of Escherichia coli. *J. Mol. Biol.* **1991**, *222*, 599−620.

(36) Minton, A. P. The Influence of Macromolecular Crowding and Macromolecular Confinement on Biochemical Reactions in Physiological Media. *J. Biol. Chem.* **2001**, *276*, 10577−10580.

(37) Neuhofer, W.; Bartels, H.; Fraek, M.-L.; Beck, F.-X. Relationship between Intracellular Ionic Strength and Expression of Tonicity-Responsive Genes in Rat Papillary Collecting Duct Cells. *J. Physiol.* **2002**, *543*, 147−153.

(38) Nunes, P.; Roth, I.; Meda, P.; Féraille, E.; Brown, D.; Hasler, U. Ionic Imbalance, in Addition to Molecular Crowding, Abates Cytoskeletal Dynamics and Vesicle Motility during Hypertonic Stress. *Proc. Natl. Acad. Sci. U. S. A.* **2015**, *112*, E3104−E3113.

(39) Lee, B. H.-j.; Arya, G. Analytical van der Waals Interaction Potential for Faceted Nanoparticles. *Nanoscale Horiz.* **2020**, *5*, 1628−1642.

(40) Moody, B. *Comparative Inorganic Chemistry*; Edward Arnold: London, 1991.

(41) Kim, T.; Lee, K.; Gong, M.-s.; Joo, S.-W. Control of Gold Nanoparticle Aggregates by Manipulation of Interparticle Interaction. *Langmuir* **2005**, *21*, 9524−9528.

(42) Israelachvili, J. N. *Intermolecular and Surface Forces*; Academic Press: New York, 2011.

(43) Stobiecka, M.; Coopersmith, K.; Hepel, M. Resonance Elastic Light Scattering (RELS) Spectroscopy of Fast Non-Langmuirian Ligand-Exchange in Glutathione-Induced Gold Nanoparticle Assembly. *J. Colloid Interface Sci.* **2010**, *350*, 168−177.

(44) Ahmad, I.; Derkink, F.; Boulogne, T.; Bampoulis, P.; Zandvliet, H. J.; Khan, H. U.; Jan, R.; Kooij, E. S. Self-Assembly and Wetting

Properties of Gold Nanorod−CTAB Molecules on HOPG. *Beilstein J. Nanotechnol.* **2019**, *10*, 696−705.

(45) Hlawacek, G.; Ahmad, I.; Smithers, M. A.; Kooij, E. S. To See or Not to See: Imaging Surfactant Coated Nano-Particles Using HIM and SEM. *Ultramicroscopy* **2013**, *135*, 89−94.

(46) Drobek, T.; Spencer, N. D.; Heuberger, M. Compressing PEG Brushes. *Macromolecules* **2005**, *38*, 5254−5259.

(47) Heuberger, M.; Drobek, T.; Spencer, N. D. Interaction Forces and Morphology of a Protein-Resistant Poly(ethylene Glycol) Layer. *Biophys. J.* **2005**, *88*, 495−504.

(48) Minton, A. P. The Effect of Volume Occupancy upon the Thermodynamic Activity of Proteins: Some Biochemical Consequences. *Mol. Cell. Biochem.* **1983**, *55*, 119−140.

(49) Ross, P. D.; Minton, A. P. Analysis of Non-Ideal Behavior in Concentrated Hemoglobin Solutions. *J. Mol. Biol.* **1977**, *112*, 437−452.

(50) Ross, P. D.; Briehl, R. W.; Minton, A. P. Temperature Dependence of Nonideality in Concentrated Solutions of Hemoglobin. *Biopolymers* **1978**, *17*, 2285−2288.

(51) Levicky, R.; Herne, T. M.; Tarlov, M. J.; Satija, S. K. Using Self-Assembly to Control the Structure of DNA Monolayers on Gold: A Neutron Reflectivity Study. *J. Am. Chem. Soc.* **1998**, *120*, 9787−9792.

(52) Lee, O.-S.; Cho, V. Y.; Schatz, G. C. A-to B-Form Transition in DNA between Gold Surfaces. *J. Phys. Chem. B* **2012**, *116*, 7000−7005.

(53) Pawlak, R.; Vilhena, J.; Hinaut, A.; Meier, T.; Glatzel, T.; Baratoff, A.; Gnecco, E.; Pérez, R.; Meyer, E. Conformations and Cryo-Force Spectroscopy of Spray-Deposited Single-Strand DNA on Gold. *Nat. Commun.* **2019**, *10*, 1−7.